International Journal of Heat and Technology
Vol. 36, No. 4, December, 2018, pp. 1212-1222
Journal homepage: http://iieta.org/Journals/IJHT

Indoor investigation and numerical analysis of PV cells temperature regulation using coupled PCM/Fins

Abdulmunem R. Abdulmunem*, Jalal M. Jalil

Electromechanical Eng. Dept., University of Technology, Baghdad 10066, Iraq

Corresponding Author Email: abdulmunemraad@yahoo.com

https://doi.org/10.18280/ijht.360408

Received: 10 April 2018
Accepted: 8 October 2018

Keywords:
numerical analysis, PV cell, PCM/Fins, temperature regulation, improved performance

ABSTRACT

This work aims at utilizing the paraffin wax (PCM) latent heat of fusion and calculates the effect of coupling aluminum fins with PCM, to regulate PV cells temperature for the sake of enhancing performance. Absorbing the heat energy from its surface was investigated experimentally and numerically. From the experimental results and the numerical simulation of the paraffin wax melting behavior inside a PV cell container in the back side with and without fins is seen by using of coupled PCM/Fins, which led to good distribution of temperature inside PCM as compared with using PCM only. The use of aluminum fins with PCM led to accelerate melting of PCM by 3.5 min at a depth of 2 cm and about 14 min at a depth of 3 cm compared with using PCM only. This led to more dropping in PV cell temperature compared with using PCM only. The percentage in PV cell temperature drop was about 18.3% by using PCM only and 27.8% by using coupled PCM/Fins compared with PV cell without additive materials (PCM). The improvement in the used PV cell performance with dropping in its temperature was about, 9.84% and 5.1% on maximum power and fill factor, respectively, with using PCM only, and about 14.19% and 7.37% on maximum power and fill factor, respectively with using coupled PCM/Fins, compared with using PV cell without PCM.

1. INTRODUCTION

Photovoltaic cells are more affected by rising in its temperature which led to dropping in the electrical power generated. There are two ways to avoid PV cells rising temperature; internally by using silicon cells to generate electricity, and externally by absorbing radiations that contained amounts of infrared. Thus the PV panels are less efficient in hot climate regions such as Middle East countries. For this reason, the need arises to regulate the PV cells temperature. One of the most important methods for regulating PV cells temperatures are the passive cooling (no need to power) by using latent heat of fusion for phase change materials (PCM) to absorb the rising in temperature from the silicon cells. There are many studies that focused on using these materials in different applications. Such as: Korti [1] solved two-dimensional numerical simulations for double-pass solar collector integrated in the lower channel with spherical PCM media. A finite volumes method was used on energy balances, momentum, and mass. It was found that the PCM spheres at the bottom absorber were the best configuration and allowed increasing in the outlet temperature. Also, it can enhance the collector thermal performance using several types of PCMs. Jung et al. [2] studied experimentally and CFD analyzed the impact on the energy storage time of the PCM in vertical cylinder with different variables such as (number of fins, materials thermal conductivity and warm water temperature supplied), the change in the number of circular fins and the warm water temperature supplied were influenced substantially by the PCM melting. The changes in the pipe, circular fins thermal conductivity is only a meager influence on the PCM melting. Huang et al. [3] presented an experimental investigation and numerical simulation using the phase change material to moderate a building integrated photovoltaic temperature rise. The study showed that the moderation of temperature achieved, can lead to significant improvements in the operational efficiency of photovoltaic facades. Hasan et al. [4] studied experimentally building temperature regulation integrated with photovoltaic panel using PCM. A reduction in maximum temperature at insolation 1000 W/m^2 of 18^{o}C for 30 min was achieved, while the reduction in temperature was 10 oC maintained for 5 h. Huang [5] developed a PV/PCM numerical simulation model for single PCM application to predict the thermal performance of the multi-PCMs in a triangular cell in the PV/PCM system. Ciulla [6] studied the PV/PCM system numerically using a finite difference model, the study focused on the assessing method for reducing the PV systems peak temperature by using Phase Change Materials. Park [7] analyzed the annual generation of electric energy on a vertical PV module with changes in the (installation direction of the system, melting temperatures and thicknesses of the PCM). The experimental results indicated that, the effect of the PCM was decreased in winter and that the optimal thickness of PCM depends on system installation direction. Browne et al. [8] shows that the PCM is the best effective way to removing heat from the PV panels, hybrid PV/T/PCM was the experimental system. The effect of using inner longitudinal fins in a rectangular encapsulation on the melting process of paraffin wax was investigated experimentally and numerically by Jalil et al. [9]. The results show that using inner longitudinal fins gives

decreasing in the temperature of absorber surface because of part of the heat are injected deeply in the PCM and gives accelerating in the PCM melting process. Abdulmunem [10] studied experimentally the effect of using aluminum foam matrix on the in the effective physical properties of PCM, such as thermal conductivities. The results indicated that using aluminum foam matrix with PCM gives good distribution of temperature inside PCM and more absorption of heat from the used PV cell. Kawtharani et al. [11] tested an organic PCM to study its properties and absorption heat capacity as a PV cooling material. The results indicated that about 13% of the heat can be saved and the ability of the PCM for absorption heat led to enhancing in the PV panel performance. Hassan et al. [12] evaluated the energy saving performance of PV-PCM system throughout the year in United Arab Emirates. PV-PCM system was employed in extremely hot environment and gives enhanced PV power output by 5.9% annually, due contributing the PCM in the system cooling.

From the previous researches, the phase change materials are new materials that can be used to absorb temperature from the hot surface and led to decrease surface temperature. Latent heat of fusion for these materials can be utilized to make these materials as passive cooling materials. This work aims to investigate numerically and experimentally the effect of using PCM with and without fins on the PV cell thermal performance.

2. METHODOLOGIES

2.1 Numerical formulations of temperature distribution inside PCM

Stefan problems are representing heat conduction problems with phase change using enthalpy transforming method, converting the energy equation to a non-linear equation by this method with single dependent variable enthalpy (L). The enthalpy method advantage is; the problem formulated in a fixed region to be solved. This method In addition to temperature treats the enthalpy as a dependent variable and discretizes the energy equation into a set of equations that contain both enthalpy and temperature. The analytical assumptions are:

1. Viscous dissipation are neglected,
2. Radiation and convection terms are neglected.
3. Specific heats are constant for each phase, where the phase change occurs at a single temperature. The analysis in three-dimensions of the model is related to Cao [13].

The equation of energy is:

$$\frac{\partial}{\partial x}\left(k\frac{\partial T}{\partial x}\right)+\frac{\partial}{\partial y}\left(k\frac{\partial T}{\partial y}\right)+\frac{\partial}{\partial z}\left(k\frac{\partial T}{\partial z}\right)+\bar{q}=\rho\frac{\partial L}{\partial t} \tag{1}$$

and the equation of state,

$$\frac{dL}{dT}=Cp \tag{2}$$

where the specific heat case for each phase is constant and the phase change occurs at a single temperature [14],

$$T=\begin{cases} T_m+L/Cp_s & l\le 0 \quad \text{(Solid phase)} \\ T_m & 0<L<l \quad \text{(Phase change)} \\ T_m+(L-l)/Cp_l & L\ge l \quad \text{(Liquid phase)} \end{cases} \tag{3}$$

For the last relation, $l = 0$ was selected to PCM (phase change material) in their solid state to temperature T_m.
The "Kirchhoff" temperature is introduced as [15]:

$$T^*=\int_{T_m}^{T}k(\eta)d\eta=\begin{cases} k_s(T-T_m), & T<T_m \\ 0, & T=T_m \\ k_l(T-T_m), & T>T_m \end{cases} \tag{4}$$

Using equation (3), equation (4) becomes:

$$T^*=\begin{cases} k_sL/Cp_{s,} & L\le 0 \\ 0, & 0<L<l \\ k_l(L-l)/Cp_{l,} & L\ge l \end{cases} \tag{5}$$

The enthalpy is introducing as a function of temperature:

$$T^*=\lambda(L)L+S(L) \tag{6}$$

For a single temperature, the phase change:

$$\lambda(L)=\begin{cases} k_s/Cp_s, & L\le 0 \\ 0, & 0<L<l \\ k_l/Cp_{l,} & L\ge l \end{cases} \tag{7}$$

and

$$S(L)=\begin{cases} 0, & L\le 0 \\ 0, & 0<L<l \\ -lk_l/Cp_{l,} & L\ge l \end{cases} \tag{8}$$

Transforming equation (1) and substituting equation (6) In terms of Kirchhoff temperature gives:

$$\rho\frac{\partial L}{\partial t}=\frac{\partial}{\partial x}\left(\frac{\partial(\lambda L)}{\partial x}\right)+\frac{\partial}{\partial y}\left(\frac{\partial(\lambda L)}{\partial y}\right)+\frac{\partial}{\partial z}\left(\frac{\partial(\lambda L)}{\partial z}\right)+p+q \tag{9}$$

With

$$p=\frac{\partial}{\partial x}\left(\frac{\partial S}{\partial x}\right)+\frac{\partial}{\partial y}\left(\frac{\partial S}{\partial y}\right)+\frac{\partial}{\partial z}\left(\frac{\partial S}{\partial z}\right) \tag{10}$$

Equation (9) is reduced to the linear energy equation for the liquid region away from the moving front:

$$\rho\frac{\partial L}{\partial t}=\frac{\partial}{\partial x}\left(k_l\frac{\partial T}{\partial x}\right)+\frac{\partial}{\partial y}\left(k_l\frac{\partial T}{\partial y}\right)+\frac{\partial}{\partial z}\left(k_l\frac{\partial T}{\partial z}\right)+q \tag{11}$$

For the solid region, Equation (9) becomes:

$$\rho\frac{\partial L}{\partial t}=\frac{\partial}{\partial x}\left(k_s\frac{\partial T}{\partial x}\right)+\frac{\partial}{\partial y}\left(k_s\frac{\partial T}{\partial y}\right)+\frac{\partial}{\partial z}\left(k_s\frac{\partial T}{\partial z}\right)+q \tag{12}$$

In the phase change region without convection term, equation (9) becomes:

$$\rho\frac{\partial L}{\partial t}=\frac{\partial^2}{\partial x^2}(\lambda L)+\frac{\partial S^2}{\partial x^2}+\frac{\partial^2}{\partial y^2}(\lambda L)+\frac{\partial S^2}{\partial y^2}+\frac{\partial^2}{\partial z^2}(\lambda L)+\frac{\partial S^2}{\partial z^2}+q \tag{13}$$

For $\lambda=\lambda(L) and S=S(L)$, the control volume finite difference employs the above equation. In this methodology, the discretization equation was obtained using conservation laws over finite-size control volume surrounding the grid nodes. Equation Integration over the control volumes as:

$$\iiint_{\Delta V}\rho\frac{\partial L}{\partial t}\Delta V=\iiint_{\Delta V}\frac{\partial}{\partial x}\left(\frac{\partial\lambda(L)}{\partial x}\right)\Delta V+\iiint_{\Delta V}\frac{\partial}{\partial y}\left(\frac{\partial\lambda(L)}{\partial y}\right)\Delta V+\iiint_{\Delta V}\frac{\partial}{\partial z}\left(\frac{\partial\lambda(L)}{\partial z}\right)\Delta V$$
$$+\iiint_{\Delta V}\frac{\partial}{\partial x}\left(\frac{\partial S}{\partial x}\right)\Delta V+\iiint_{\Delta V}\frac{\partial}{\partial y}\left(\frac{\partial S}{\partial y}\right)\Delta V+\iiint_{\Delta V}\frac{\partial}{\partial z}\left(\frac{\partial S}{\partial z}\right)\Delta V$$
$$+\iiint_{\Delta V}q\Delta V \tag{14}$$

using an explicit scheme: The time variation term becomes:

$$\iiint_{\Delta V}\rho\frac{\partial L}{\partial t}\Delta V=\rho\Delta V\left(\frac{L_p-L_p^{\circ}}{\Delta t}\right) \tag{15}$$

In x-direction the right side of equation (14) becomes:

$$\iiint_{\Delta V}\frac{\partial}{\partial x}\left(\frac{\partial\lambda(L)}{\partial x}\right)\Delta V=\left[\left(\frac{\partial\lambda(L)}{\partial x}\right)_e-\left(\frac{\partial\lambda(L)}{\partial x}\right)_w\right]\Delta y\,\Delta z$$
$$=\frac{\Delta y\Delta z}{(\delta x)_e}\left(\lambda_E L_E-\lambda_p L_p\right)-\frac{\Delta y\Delta z}{(\delta x)_w}\left(\lambda_p L_p-\lambda_W L_W\right) \tag{16}$$

$$\iiint_{\Delta V}\frac{\partial}{\partial x}\left(\frac{\partial S}{\partial x}\right)\Delta V=\left[\left(\frac{\partial S}{\partial x}\right)_e-\left(\frac{\partial S}{\partial x}\right)_w\right]\Delta y\,\Delta z$$
$$=\frac{\Delta y\,\Delta z}{(\delta x)_e}\left(S_E-S_P\right)-\frac{\Delta y\,\Delta z}{(\delta x)_w}\left(S_P-S_W\right) \tag{17}$$

In *y*-direction, the right side of equation (14) becomes:

$$\iiint_{\Delta V}\frac{\partial}{\partial y}\left(\frac{\partial\lambda(L)}{\partial y}\right)\Delta V=\left[\left(\frac{\partial\lambda(L)}{\partial y}\right)_n-\left(\frac{\partial\lambda(L)}{\partial y}\right)_s\right]\Delta x\,\Delta z$$
$$=\frac{\Delta x\Delta z}{(\delta y)_n}\left(\lambda_N L_N-\lambda_p L_P\right)-\frac{\Delta x\Delta z}{(\delta y)_S}\left(\lambda_p L_P-\lambda_S L_S\right) \tag{18}$$

$$\iiint_{\Delta V}\frac{\partial}{\partial y}\left(\frac{\partial S}{\partial y}\right)\Delta V=\left[\left(\frac{\partial S}{\partial y}\right)_n-\left(\frac{\partial S}{\partial y}\right)_s\right]\Delta x\Delta z$$
$$=\frac{\Delta x\Delta z}{(\delta y)_n}\left(S_N-S_P\right)-\frac{\Delta x\Delta z}{(\delta y)_s}\left(S_P-S_S\right) \tag{19}$$

And In z-direction, the right side of equation (14) becomes:

$$\iiint_{\Delta V}\frac{\partial}{\partial z}\left(\frac{\partial\lambda(L)}{\partial z}\right)\Delta V=\left[\left(\frac{\partial\lambda(L)}{\partial z}\right)_t-\left(\frac{\partial\lambda(L)}{\partial z}\right)_b\right]\Delta x\,\Delta y$$
$$=\frac{\Delta x\Delta y}{(\delta z)_t}\left(\lambda_T L_T-\lambda_P L_P\right)-\frac{\Delta x\Delta y}{(\delta z)_b}\left(\lambda_P L_P-\lambda_B L_B\right) \tag{20}$$

$$\iiint_{\Delta V}\frac{\partial}{\partial z}\left(\frac{\partial S}{\partial z}\right)\Delta V=\left[\left(\frac{\partial S}{\partial z}\right)_t-\left(\frac{\partial S}{\partial z}\right)_b\right]\Delta x\Delta y$$
$$=\frac{\Delta x\Delta y}{(\delta z)_t}\left(S_T-S_P\right)-\frac{\Delta x\Delta y}{(\delta z)_b}\left(S_p-S_B\right) \tag{21}$$

The last term from right side of equation (14) becomes

$$\iiint_{\Delta V}q\Delta V=\bar{q}\,\Delta V, \tag{22}$$

Now, let a_N, a_S, a_E, a_W, a_T *and* a_B be the coefficients of L_N, L_S, L_E, L_W, L_T and L_B, respectively. Equation (15) becomes in the standard form:

$$a_P L_P=a_N L_N+a_S L_S+a_E L_E+a_W L_W+a_T L_T+a_B L_B+b \tag{23}$$

The old value of L at grid point P denoting by L_p^o , the coefficients values are:

$$a_p=a_N+a_S+a_W+a_E+a_T+a_B$$

$$a_E=\frac{\Delta t}{\rho\Delta V}\frac{\lambda_E A_x}{\delta x_e},a_W=\frac{\Delta t}{\rho\Delta V}\frac{\lambda_W A_x}{\delta x_w},a_N=\frac{\Delta t}{\rho\Delta V}\frac{\lambda_N A_y}{\delta y_n},$$
$$a_S=\frac{\Delta t}{\rho\Delta V}\frac{\lambda_S A_y}{\delta y_s},a_T=\frac{\Delta t}{\rho\Delta V}\frac{\lambda_T A_z}{\delta z_t},a_B=\frac{\Delta t}{\rho\Delta V}\frac{\lambda_B A_z}{\delta z_b} \tag{24}$$

$$A_x=\Delta y\Delta z,A_y=\Delta x\Delta z,A_z=\Delta x\Delta y,\Delta V=\Delta x\Delta y\Delta z$$

and,

$$b=-\left[a_N+a_S+a_E+a_W+a_T+a_B-1\right]L_P^{\circ}+b_N S_N+b_S S_S+b_E S_E+b_W S_W+b_T S_T+$$
$$b_B S_B-b_P S_P+\frac{dt}{\rho}q\Delta V \tag{25}$$

In which,

$$b_P=b_E+b_W+b_S+b_N+b_T+b_B$$
$$b_E=\frac{\Delta t}{\rho\Delta V}\frac{A_x}{\delta x_e},b_W=\frac{\Delta t}{\rho\Delta V}\frac{A_x}{\delta x_w},b_N=\frac{\Delta t}{\rho\Delta V}\frac{A_y}{\delta y_n},b_S=\frac{\Delta t}{\rho\Delta V}\frac{A_y}{\delta y_s} \tag{26}$$

For solid and liquid regions, the last procedure is similar for equations (11) and (12). In x, y, and z directions, The Cartesian mesh is 31*11*11 and the time step is 1 second. Grid independence was tested by using finer mesh where the difference in temperature results was less than 1 ^{o}C.

2.1.1 Numerical solution

The numerical scheme solves the conduction problem in wax with phase change. The results of the numerical solution were the enthalpy and temperature values in three dimensional Cartesian coordinates. The numerical scheme divides the two phase wax into three distinct regions. First one is the pure solid (in case all neighbor nodes were solid), the second one is the pure liquid (in case all neighbor nodes were liquid) and third one is the mushy region (in case neighbor nodes were mixed). The value of enthalpy in the node can decide the phase of the node. For solid and liquid regions, normal conduction equations were used while in the mushy region, a special equation was used.

2.2 PV cell electrical performance

The electrical performance of PV cells can be found by using [16-18]

$$FF = \frac{P_{max}}{I_{sc} \times V_{oc}} \quad (27)$$

Where:

$$P_{max} = I_{mpp} \times V_{mpp} \quad (28)$$

Then the electrical efficiency of PV panel (η_{el}) is:-

$$\eta_{el} = \frac{P_{max}}{G \times A_{PV}} \quad (29)$$

3. EXPERIMENTAL PART

3.1 System configuration

The traditional PV panels consist of many individual PV cells. These cells are connected during manufacturing in parallel and series products. Large sized panels are manufactured according to the amount of power needed. In this work, the system was constructed and analyzed as individual PV cells, to show the effect of rising temperature while, using materials (PCM and Fins) as passive cooling materials on PV cell power generation. The construction test model consists of (13.5 cm x 13.5 cm) mono-crystalline silicon PV cells with (1.6 Watt) maximum power at ideal conditions (G = 1000 W/m^2, T = 25 ^{o}C), this cell is coupled in the back side with the same dimensions of aluminum plate of (1mm) thickness, welded with three aluminum fins (13 cm x 4 cm) x (1mm) thickness. High thermal conductivity heat sink paste was used in the back surface of PV cell, to close the air gap and ensure heat transfer from PV cell to fins. The PCM container was made from wood material with dimensions (13 cm length x 13 cm width x 4 cm depth) and slather with R.T.V silicon to avoid drainage of the PCM during the melting process. The tests were done indoors, to show the effect of rising temperature on the test model under constant irradiance, and to eliminate the changes in the environment such as wind speed, etc. Sun simulator consists of 500 W halogen solar lamps at a distance of 40 cm to give irradiation of 800 W/m^2. In the first test case, the model was tested without using materials (PCM and fins). The second test case, the PCM container was filled with PCM (specified in Table 1) to show the effect of using this material on PV cell temperature. Low thermal conductivity of paraffin wax as shown in Table 1 led to trying to use fins in the third test case; to dissipate heat deeply inside PCM. Figure 1 shows the experimental configuration.

Table 1. Paraffin wax specifications

Parameter	Value
Density (kg/m^3)	Solid(880)/ Liquid(760)
Thermal conductivity (W/m K)	Solid(0.24)/ liquid(0.22)
Specific heat (kJ/kg K)	Solid (2.9)/ Liquid (2.2)
Latent heat (kJ/kg)	142
Melting temperature (deg.C)	42

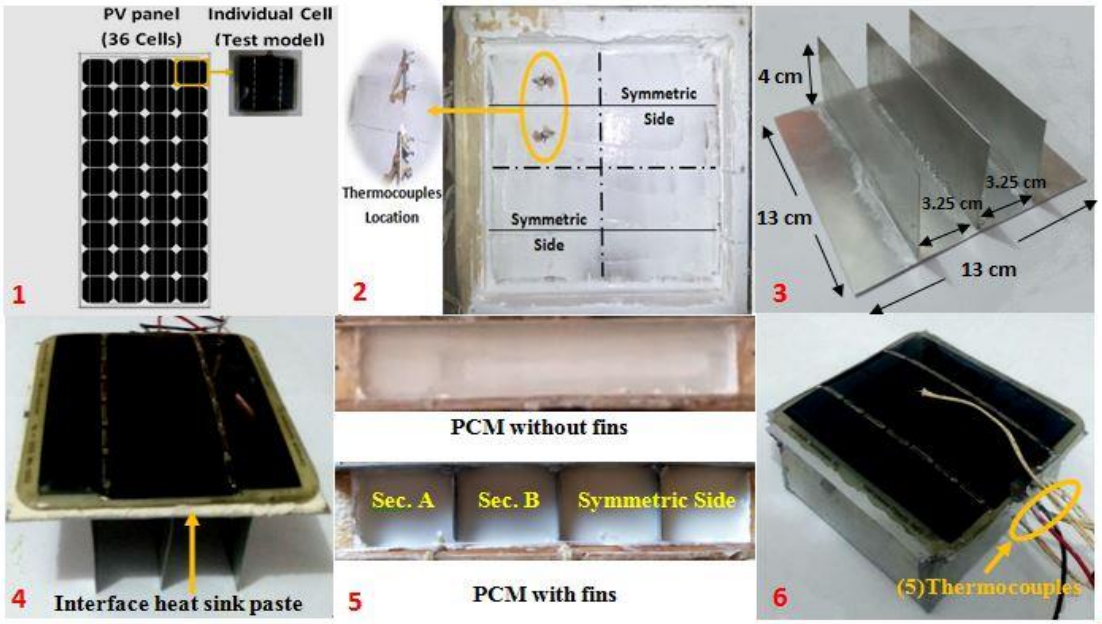

Figure 1. Experiment configuration

3.2 Experimental measurements

The tests were done in laboratories of renewable energy in University of Technology/Electromechanical Eng. Dept. Five thermocouples were connected to the thermo recorder to measuring the temperatures' at a different distance inside PCM, three thermocouples was inserted at a depth of 1 cm, 2 cm and 3 cm inside PCM. While other two thermocouples were placed in front and rear PV cell surfaces to give average PV cell temperature. Light intensity sensor was used to measuring the irradiance intensity. To show the temperature distribution inside paraffin wax with melting process, the infrared camera was used for this purpose. A digital electrical board was used to measure the electrical output of the PV cell. The used instruments in this work and its accuracy are listed in Table 2. Figure 2 shows complete system with the schematic diagram of this work.

Table 2. Instruments used

Instrument	Type	Accuracy
Digital thermo recorder	TM-946	±0.02%
Thermocouples	K	±0.4%
Light intensity sensor	Protek / DM301	±0.7%
Infrared camera	Fluke-Ti300	±2%
Digital electrical measuring board	DL9021	±0.2%

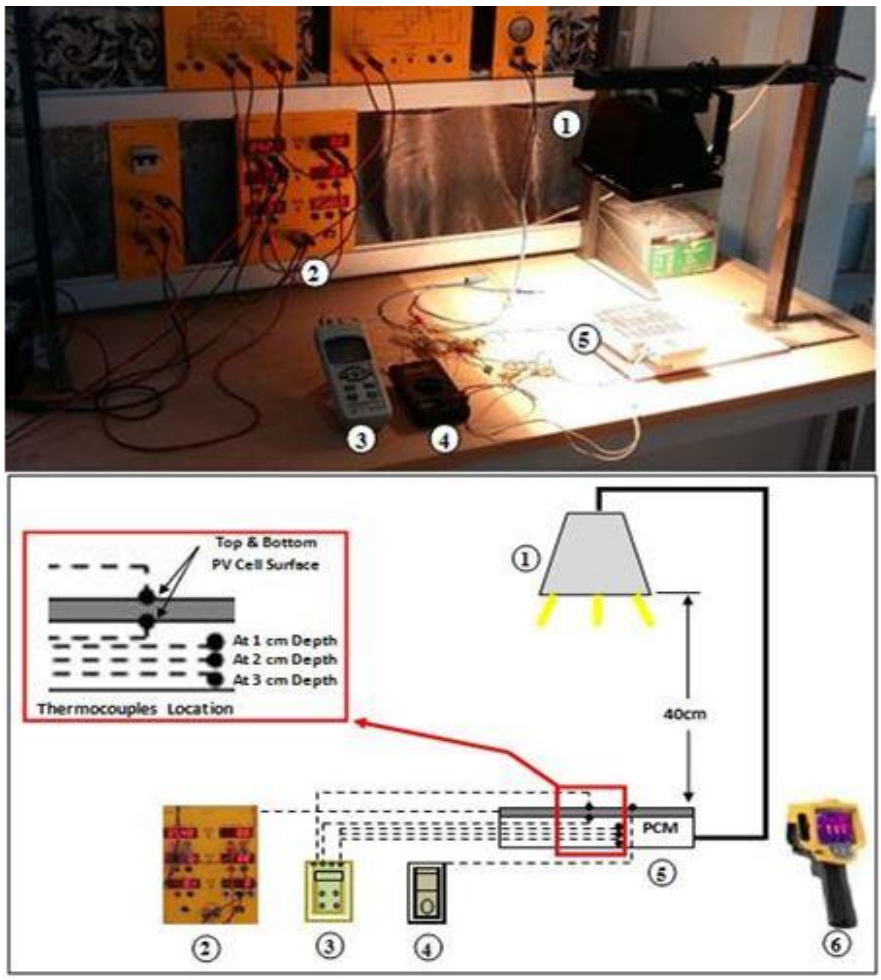

Figure 2. System configuration with schematic diagram, 1- Sun simulator, 2- Electrical measurement board, 3- Digital thermo recorder, 4- Light intensity meter, 5- Test model, 6- Infrared Camera**.**

3.3 Uncertainty analysis for the measured values

The difference between the real and measured values for any variable are defined an error. By computing the error values, the uncertainty will be identified. In this work, it can be estimate the uncertainties for the measured values using the general formula [19]

$$U = \sqrt{(\partial R/\partial v_1 * E_1)^2 + (\partial R/\partial v_2 * E_2)^2 + \cdots + (\partial R/\partial v_n * E_n)^2} \quad (30)$$

where R is a given function of the independent variables v_1, v_2 to v_n, with **U** the uncertainty in the result E_1, E_2 to E_n, represents the uncertainties of each independently measured variable as shown in table 3.

Table 3. Measured variable uncertainties

Parameters	Quantity	Uncertainty (U)
Irradiance	(G)	2%
Temperature	(T)	1°C
Voltage	(V)	0.5%
Current	(I)	0.5%

4. RESULTS AND DISCUSSION

4.1 Numerical model validation

The grid dependence was studied using three sets of grid sizes in the y and z directions. The y and z directions represent the temperature change directions. The three grid sizes were 11*11, 15*15 and 21*21. The results for temperature at a depth 1 cm inside PCM are shown in the Figure 3. The results in this figure represent one case only (PCM without fins). The chosen scheme was 11*11 because the maximum temperature difference between 15*15 and 11*11 grids is 0.73 °C, and between 21*21 and 15*15 grids is 1.36 °C, so the 11*11 results represents acceptable accuracy and no finer grids were needed.

After deciding the grid sizes, a time step was needed to achieve the stable condition. Normally the time step depends on grid sizes and properties of the materials. For the materials used in this study and mesh sizes 31*11*11, the stable time step was found equals to 1 sec.

A numerical simulation of the paraffin wax melting behavior with and without fins, inside the PV cell back side container are taken using a FORTRAN (F90) Language. The comparison between experimental (infrared camera photographs) for the used a rectangular container of PV cell, and numerical simulation results are shown in Figure 4 (a and b). It seen that; using the coupled PCM/Fins led to good distribution of temperature inside PCM comparative with PCM only as shown, because of the low thermal conductivity of the PCM material (Table1) led to that the temperature taking a long time to transfer inside the PCM, and using aluminum fins led to inject heat energy deeply in side paraffin wax (PCM). The numerical results show a good agreement with the experimental, they show a satisfactory error ratios fluctuated between 6% and 8 % along the test time (35 minute), which usually acceptable in contours plots.

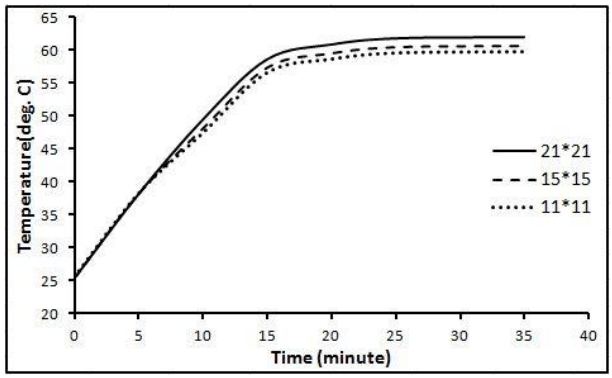

Figure 3. Grid independence study

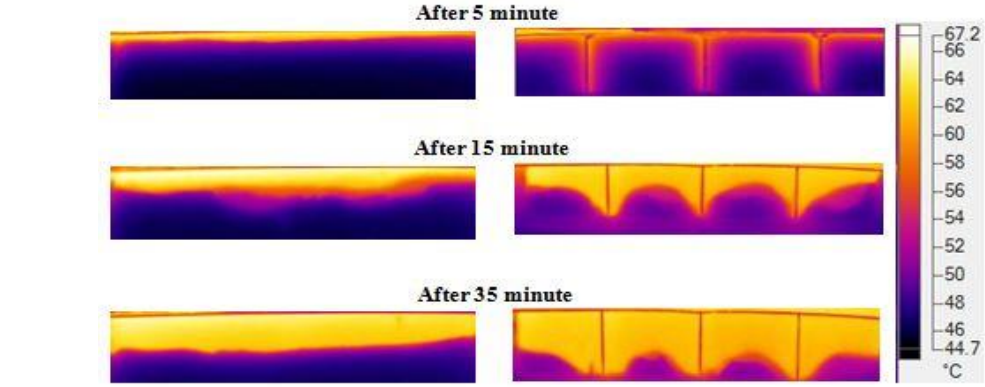

(a)

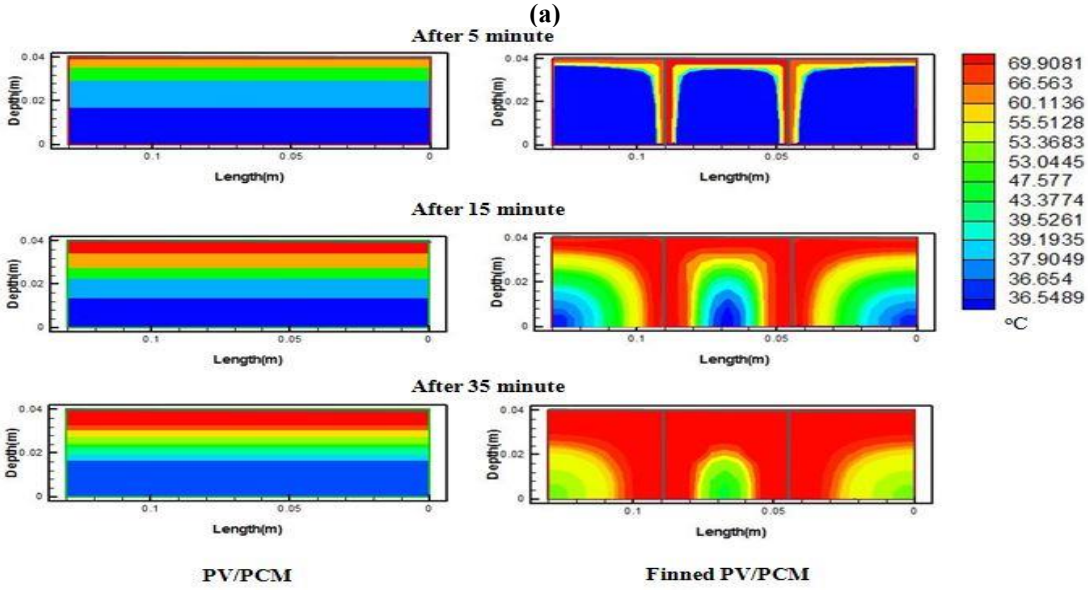

(b)

Figure 4. Temperature distribution inside PCM with and without fins, a- Infrared photographs b- Numerical simulation

4.2 PCM incorporation

The thermocouples reading for both PV cell's containers (with and without PCM) are shown in Figures 5 and 6, respectively. Figure 5 shows that the PV cell temperature for the container without PCM is higher than the other by about 13.4 ºC at the end of the test. That is because the heat energy was absorbed by the paraffin wax and this leads to dropping in the PV cell temperature.

Figure 6 shows that the temperatures distribution and PCM melting behavior at a distance of 1, 2 and 3 cm inside PV cell container without fins along test time, it was seen that at the test end the difference between the PCM temperature at a depth of 1 and 2 cm was 17 ºC and about 13.5 ºC between the PCM temperature at a depth of 2 and 3 cm. This temperature difference at the same depths was compared with using aluminum fins in section 3.3, to show the effect of using fins.

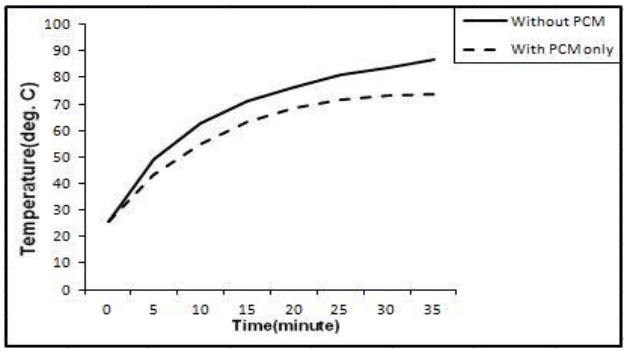

Figure 5. Comparison of PV cell temperatures with and without PCM

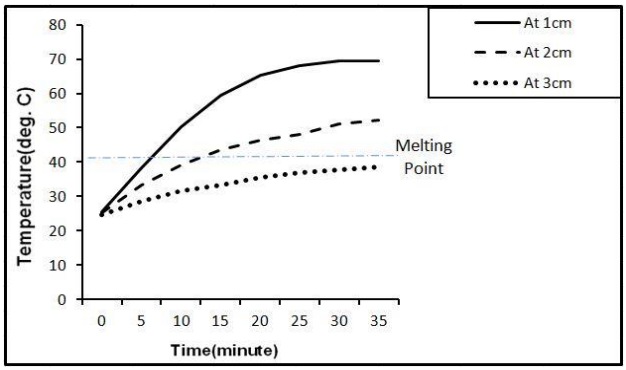

Figure 6. Thermocouples reading at different depth inside PCM

4.3 Aluminum fins effect

Figure 7 shows a comparison between two test cases, it seen that the dropping in PV cell temperature with combined PCM/fins is about 19ºC, while it was 13.5ºC with using PCM only at the end of the test, because of the low thermal conductivity of the PCM material, see (Table 1). This led to that, the temperature is taking a long time to transfer inside the PCM, and using aluminum fins led to inject heat energy deeply in side paraffin wax (PCM) as shown in Figures 3 and 4. Figure 8 shows the percentage of dropping in PV cell temperature was about 18.3% by using PCM only and 27.8% by using coupled PCM/Fins compared with PV cell without additive materials (PCM).

Figure 9 shows the temperatures distribution at a distance 1, 2 and 3 cm inside PCM with time for PV cell container with fins. It's noted that, the curves are closer in comparison with curves in Figure 6 at the same distance. The difference between the PCM temperature at depth 1 and 2 cm at the test end was 8.3ºC and about 8.7ºC between the PCM temperature at depth 2 and 3 cm. That is because of the enhancement in the temperature distribution inside PCM with using aluminum fins. In other words from the comparison between Figures 6 and 9, the advantage of using fins was that PCM melting was accelerated by 3.5 min at the depth of 2 cm and about 14 min at a depth of 3 cm. This injected heat inside PCM led to dropping in PV cell temperature.

The comparison between section A and section B for the PV cell container with fins are shown in Figures 10, 11, and 12. It is seen that, the temperature at a distance 1, 2 and 3 cm inside PCM in section B was higher than the temperature in section A. This behavior is because; at section B the paraffin wax (PCM) was affected by fins from two sides in addition to PV cell surface, but at section A, the paraffin wax was affected by one side of fins with PV cell surface.

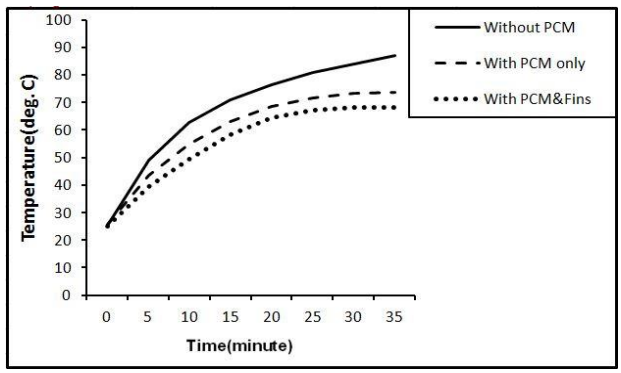

Figure 7. Comparison of PV cell temperatures

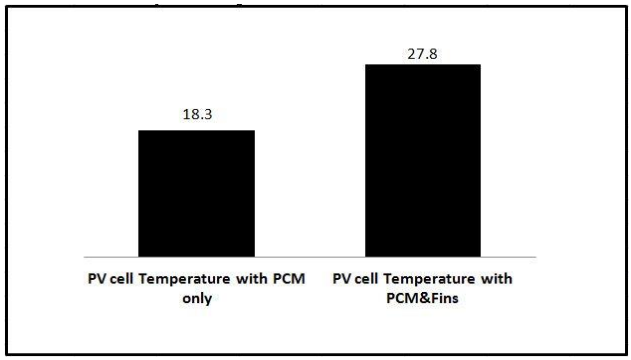

Figure 8. Percentage of PV cell temperature dropping

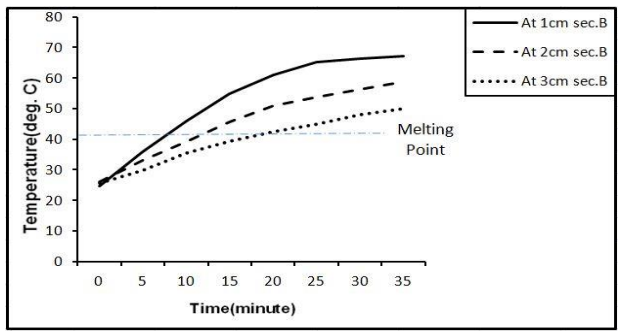

Figure 9. Variation of temperatures with time at different distance inside PCM

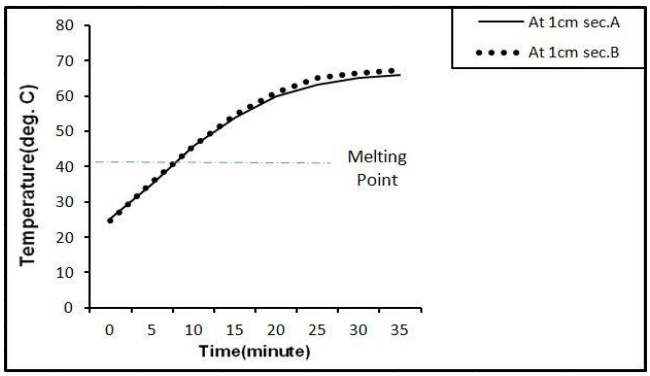

Figure 10. Variation of temperatures with time at 1 cm in sections A and B

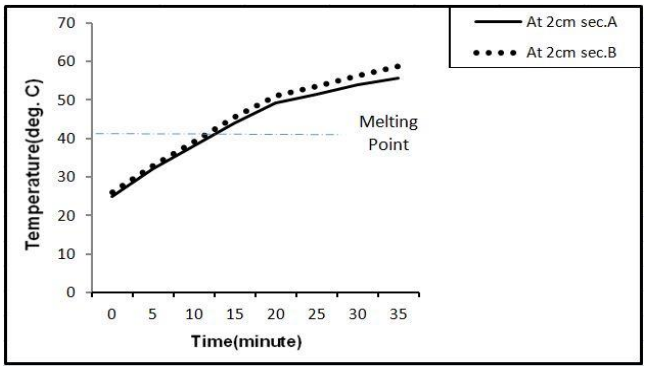

Figure 11. Variation of temperatures with time at 2 cm in section A and B

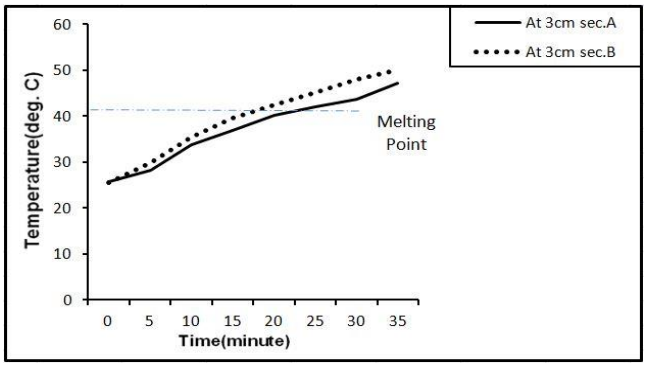

Figure 12. Variation of temperatures with time at 3 cm in section A and B

4.4 PV cell Electrical performance

Silicon PV cells are more affected by their temperature; from this work, it can be summarized that the percentage enhancement in the overall PV cell electrical performance for the two test cases in Figure 13. It is seen that from Figures 14 and 15, the increase in PV cell temperature led to decrease in both V_{oc} and $V_{mpp.}$ because; rising in temperature led to reduce in the band gap of a semiconductor (silicon cells), and the reduction in this band gap led to increase the electrons energy, therefore the need for lower energy to break the bond. In the semiconductor bond model of a band gap, reduction in the bond energy also reduces the band gap. Therefore, increasing the temperature reduces the band gap [20]. The use of PCM and PCM/Fins led to enhance these values by regulation of cell temperature as shown in Figure 13.

It can be seen from Figures 16 and 17, the increasing in PV cell temperature led to slightly increase Isc and Impp and, the main effect of rising temperature was on V_{oc} and V_{mpp}. Figure 18 shows the improvements in the maximum power generated from using PV cell, the percentage improvement in the maximum power was about 9.84% by using PCM only and about 14.19% by using coupled PCM/fins as shown. Figure 19 (a, b and c) shows the changes in I-V and P-V curves for three test cases at the test end comparison with the case without PCM. The increasing in PV cell fill factor (FF) depending on Equation 27 is shown in Figure 20, the percentage increasing in PV cell fill factor at the test end was 5.1% by using PCM only, and it was about 7.37% by using coupled PCM/fins.

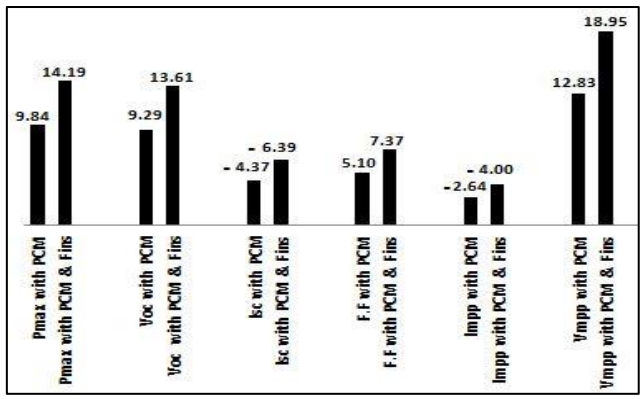

Figure 13. Percentage of PV cell enhancing performance

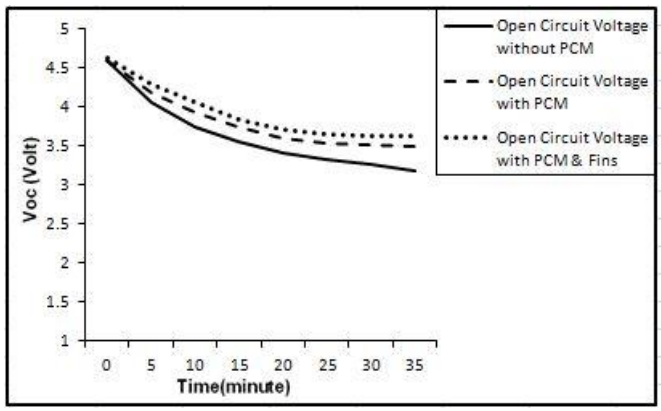

Figure 14. PV cell open circuit voltage

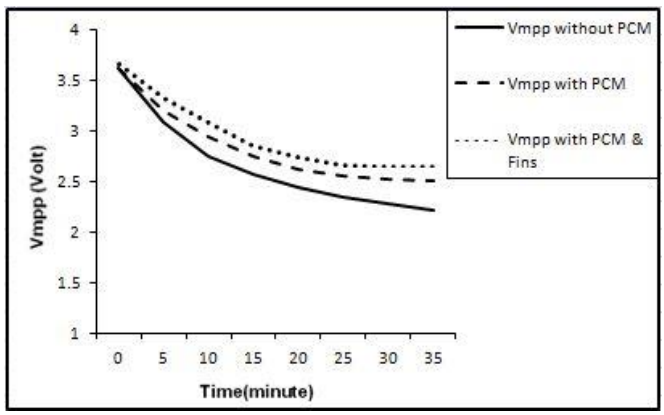

Figure 15. PV cell maximum voltage

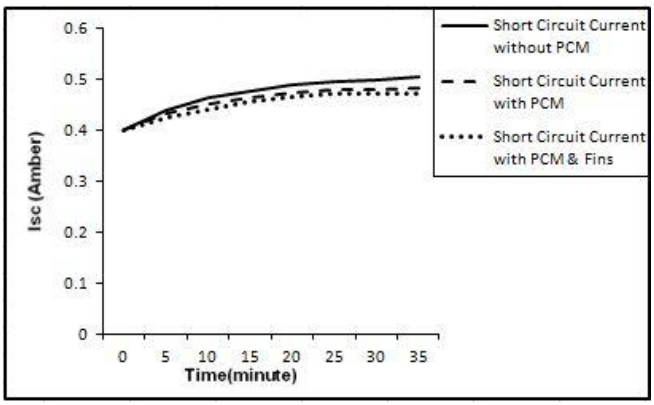

Figure 16. PV cell sort circuit current

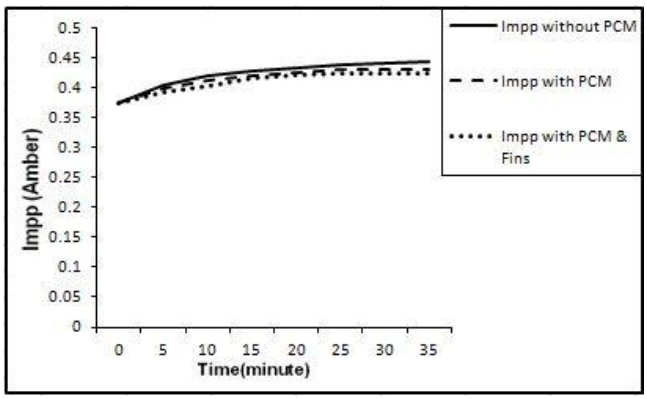

Figure 17. PV cell maximum current

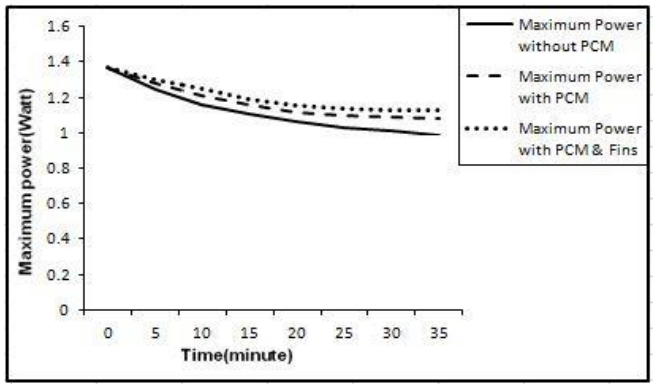

Figure 18. PV cell maximum power

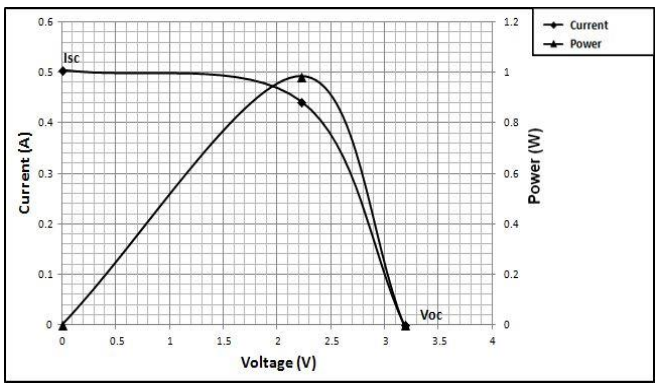

(a)

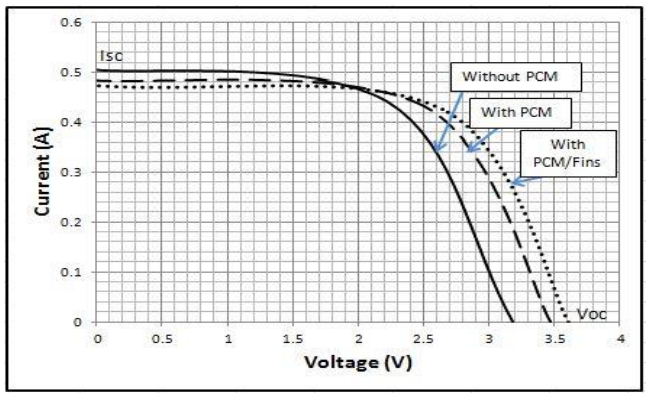

(b)

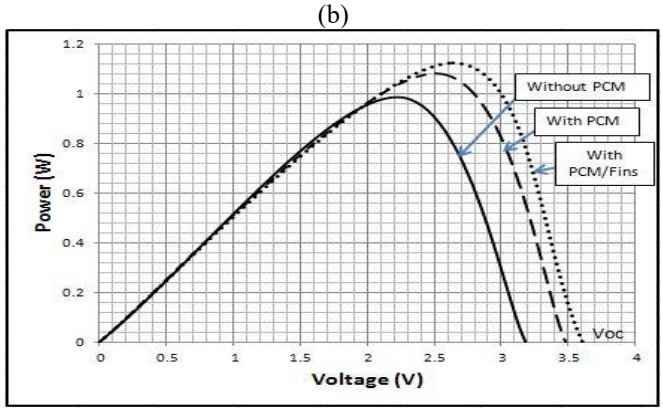

(C)

Figure 19. (a)I-V, P-V curve for PV cell without PCM at the test end, (b)The changes in I-V curve at the test end, (c) The changes in P-V curve at the test end

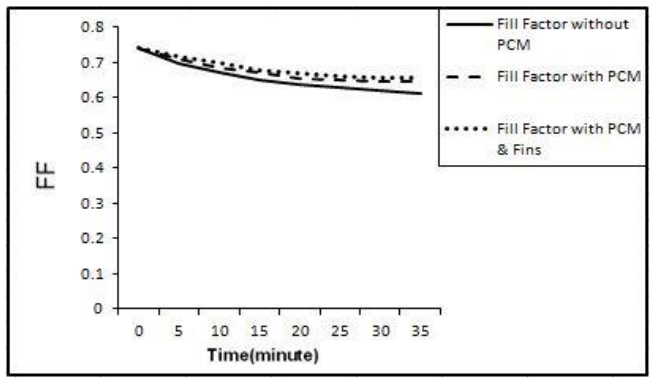

Figure 20. PV cell fill factor

5. CONCLUSIONS

This work solves the problem of high temperature in PV due to excess in solar energy in mid-day by storing it in PCM so this will improve the of electricity generation. The storing energy will be released in night time so the electricity generation will continue during the night. The fins will enhance the heat transfer process in and out of PCM. All these improvements were expressed in this work in clear numbers so the researchers can benefit potentially from this work.

From this work it can be concluded that:

Paraffin wax's latent heat of fusion can be utilized to regulate the PV cells temperature, by absorbing the heat energy from these cells. Using Aluminum fins coupled with PCM led to decrease the melting time of the PCM material

(paraffin wax) in the deep locations. While, using Aluminum fins inside the PCM led to good distribution of temperature inside the PCM and led to more absorption of temperature from the PV cell. This dropping in PV cell temperature by using these materials led to enhancement in PV cell electrical performance.

The use of aluminum fins with PCM led to accelerate melting of PCM by 3.5 min at a depth of 2 cm and about 14 min at a depth of 3 cm compared with using PCM only. This led to more dropping in PV cell temperature compared with using PCM only. The percentage in PV cell temperature drop was about 18.3% by using PCM only and 27.8% by using coupled PCM/Fins compared with PV cell without additive materials (PCM). The improvement in the used PV cell performance with dropping in its temperature was about, 9.84% and 5.1% on maximum power and fill factor, respectively, with using PCM only, and about 14.19% and 7.37% on maximum power and fill factor, respectively with using coupled PCM/Fins, compared with using PV cell without PCM.

REFERENCES

[1] Korti AIN. (2016). Numerical heat flux simulations on double pass solar collector with PCM spheres media. International J. of Air-Conditioning and Refrigeration 24: 2-15. https://doi.org/10.1142/S2010132516500103

[2] Jung UH, Ki, Kim JH, Peck JH, Kang CD, Choi YS. (2016). Numerical investigation on the melting of circular finned PCM system using CFD & full factorial design. J. of Mechanical Science and Technology 30(6): 2813-2826. https://doi.org/10.1007/s12206-016-0541-7.

[3] Huang MJ, Eames PC, Norton B. (2004). Thermal regulation of building-integrated photovoltaics using phase change materials. International J. of Heat and Mass Transfer 47: 2715-2733. https://doi.org/10.1016/j.ijheatmasstransfer.2003.11.015

[4] Hasan A, McCormack SJ, Huang MJ, Norton B. (2010). Evaluation of phase change materials for thermal regulation enhancement of building integrated photovoltaics. Solar Energy 84: 1601-1612. https://doi.org/10.1016/j.solener.2010.06.010

[5] Huang MJ. (2011). The effect of using two PCMs on the thermal regulation performance of BIPV systems. Solar Energy Materials & Solar Cells 95: 957-963. Doi:10.1016/j.solmat.2010.11.032

[6] Ciulla G, Brano VL, Cellura M, Franzitta V, Milone D. (2012). A finite difference model of a PV-PCM system. Energy Procedia 30: 198-206. https://doi.org/10.1016/j.egypro.2012.11.024

[7] Park J, Kim T, Leigh SB. (2014). Application of a phase change material to improve the electrical performance of vertical-building-added photovoltaics considering the annual weather conditions. Solar Energy 105: 561-574. https://doi.org/10.1016/j.solener.2014.04.020

[8] Browne MC, Norton B, McCormack SJ. (2016). Heat retention of a photovoltaic/thermal collector with PCM. Solar Energy 133: 533-548. https://doi.org/10.1016/j.solener.2016.04.024

[9] Jalil JM, Abdulmunem, Abdulmunem R, Abed AH. (2016). Numerical and experimental investigation of using inner longitudinal fins in a rectangular encapsulation on the PCM melting behaviors. Journal of Engineering and Sustainable Development 20(03): 139-154.

[10] Abdulmunem AR. (2017). Passive cooling by utilizing the combined PCM / aluminum foam matrix to improve solar panels performance: indoor investigation. The Iraqi Journal for Mechanical and Material Engineering 17(4) Dec.

[11] Kawtharani F, Kawtharani A, Hammoud M, Hallal A, Shaito A, Assi A, Assi I. (2017). Cooling PV modules using phase change material. IEEE, 29th International Conference on Microelectronics (ICM). https://doi.org/10.1109/ICM.2017.8268830

[12] Hassan A, Sarwar J, Alnoman H, Abdelbaqi S. (2017). Yearly energy performance of a photovoltaic-phase change material (PV-PCM) system in hot climate. Solar Energy 146: 417–429. https://doi.org/10.1016/j.solener.2017.01.070

[13] Cao, Faghri. (1989). A numerical analysis of Stefan problems for generalized multi-dimensional phase change structure using the enthalpy transformation model. J. Heat Mass Transfer 32(7): 1289-1298. https://doi.org/10.1016/0017-9310(89)90029-X

[14] Norton T, Delgado A, Hogan E, Grace P. (2009). Simulation of high pressure freezing processes by enthalpy method. J. Food Engineering 91: 260-268. https://doi.org/10.1016/j.jfoodeng.2008.08.031

[15] Cho S, Sunderland J. (1962). Heat-conduction problems with melting or freezing. J. Heat Transfer 421-425. https://doi.org/10.1115/1.3580205

[16] Cox CH, Raghuraman P. (1985). Design consideration for flat plat photovoltaic/thermal collectors. Solar Energy 35: 227-241. https://doi.org/10.1016/0038-092X(85)90102-1

[17] Hussien HA, Noman AH, Abdulmunem AR. (2015). Indoor Investigation for Improving the Hybrid Photovoltaic /Thermal System Performance Using Nanofluid (AL_2O_3-Water). Engineering & Technology Journal 33(Part (A).4): 889-901.

[18] Hussien HA, Noman AH, Abdulmunem AR. (2015). Improving of the photovoltaic/thermal system performance using water cooling technique. IOP Conference Series: Materials Science and Engineering, IOP Publishing. https://doi.org/10.1088/1757-899X/78/1/012020

[19] Guideline A. Guide engineering analysis of experimental data. Guideline 2-1986 (RA96).

[20] Duffie JA, Beckman WA. (2013). Solar engineering of thermal processes. 4th Edition by John Wiley & Sons. https://doi.org/10.1002/9781118671603

[21] Komolafe A, Waheed MA. (2018). Design and fabrication of a forced convection solar dryer integrated with heat storage materials. Revue des Composites et des Matériaux Avancés 42(1): 23-39. https://doi.org/10.3166/acsm.42.23-39.

NOMENCLATURE

A = area (m^2).
a, b = coefficient in the discretization equation
Cp = specific heat (kJ/kg. K).
E=‘east' neighbor of grid P
FF= Fill factor.
G= Irradiation (W/m^2).

I= PV cell current (A).
k =thermal conductivity (W/ m.K).
L=Enthalpy (kJ/kg)
l=latent heat (kJ/kg)
P= power (W).
PCM=Phase change material.
q=Heat generation (W/m^3)
$\bar{q}$= Average heat generation
T =Temperature (°C).
T* =Kirchhoff temperature (°C)
t =Time(s)
V= PV cell voltage (V).
V= Volume (m^3)
η = PV efficiency (%).
ρ =Density (kg/m^3).
λ = Diffusion coefficient
Δ =Difference
∂ =Partial derivative
ΔT =Temperature range (°C)
Δx , Δy , Δz = x, y, z - Direction width of the control volume
δx , δy , δz =x, y, z -direction distance between two adjacent grid points

Subscripts

B=‘bottom' neighbor of grid P
b=Control-volume face between P and B
e= Control-volume face between P and E
el= electrical
i, j, k=Unit vector
l = liquid phase
m=melting
max= Maximum
mpp= maximum power point
N=‘north’ neighbor of grid P
n=Control-volume face between P and N
OC= open circuit
P=Grid point
PV= photovoltaic panel
S= solid phase
S=‘south’ neighbor of grid P
s=Control-volume face between P and S
SC=short circuit
T=‘Top’ neighbor of grid P
t=Control-volume face between P and T
w=Control-volume face between P and W
W=west’ neighbor of grid P
x, y, z =Cartesian coordinates(m)
.